scientific reports

Check for updates

OPEN

From Khoi-San indigenous knowledge to bioengineered CeO_2 nanocrystals to exceptional UV-blocking green nanocosmetics

N. Ditlopo[1,2]✉, N. Sintwa[1,2], S. Khamlich[1,2], E. Manikandan[1,2,3], K. Gnanasekaran[1,2,4], M. Henini[1,2,5], A. Gibaud[1,2,6], A. Krief[1,2,7] & M. Maaza[1,2]✉

Single phase CeO_2 nanocrystals were bio-synthesized using Hoodia *gordonii* natural extract as an effective chelating agent. The nanocrystals with an average diameter of $\langle Ø \rangle$ ~ 5–26 nm with 4^+ electronic valence of Ce displayed a remarkable UV selectivity and an exceptional photostability. The diffuse reflectivity profile of such CeO_2 exhibited a unique UV selectivity, in a form of a Heaviside function-like type profile in the solar spectrum. While the UV reflectivity is significantly low; within the range of 0.7%, it reaches 63% in the VIS and NIR. Their relative Reactive Oxygen Species (ROS) production was found to be < 1 within a wide range of concentration (0.5–1000 µg/ml). This exceptional photostability conjugated to a sound UV selectivity opens a potential horizon to a novel family of green nano-cosmetics by green nano-processing.

Known to the Khoi and the San communities of Southern Africa, the Hoodia *gordonii* first, described by botanist R. Sweet in Hortus Britannicus in 1830[1], is a succulent plant from the Apocynaceae family (Fig. 1a). It is indigenous to South Africa and Namibia. It exhibits a significant tolerance to harsh conditions and grows in extreme environments of heat (40 °C) to low temperatures (− 3 °C). Within the modern obesity health problem, this indigenous plant has attracted a noteworthy pharmaceutical interest as per its proven traditional usage by the Khoi-San community as an appetite and thirst effective suppressant. Several bioactive compounds have been identified and isolated from its natural extract. The major bioactive compound consists of a group of glycosides, especially the one referred to as steroidal glycoside and its collective analogs such as the so called P57 which chemical structure is given in Fig. 1b. Considering the potential aldehyde components within its bioactive compounds, its natural extract is likely to be effective as an efficient chelating agent for bio-engineering nanoscaled oxides[2,3] such as Cerium oxide (CeO_2) (Fig. 1c).

The focus on such a multifunctional Cerium oxide[4–9] in this contribution is geared towards investigating its UV filtering selectivity in the perspective of designing a novel family of green nanocosmetics by an entirely green chemistry and green nano-processing. CeO_2's wide band gap (E_g: 3.0–3.6 eV) and its relatively high refractive index (n: 2.2–2.8) substantiate its application in UV radiations protection sunscreens[10–13] minimizing the risk of melanoma, sunburns and premature ageing as well as skin malignancy and related tumors.

Within this contribution, it is reported that biosynthesized CeO_2 nanocrystals using Hoodia *gordonii* natural extract as a chelating agent exhibit an exceptional UV selectivity in the 3 UV range quasi-similar to a quasi-perfect UV selectivity response with a negligible ROS factor. With such a UV selectivity and photostability, the current bio-synthesized CeO_2 nano-powder would, likely, open the horizon for a novel green UV blocking biocompatible nano-sunscreen family. Indeed, as schematically reported in Fig. 2a, the solar UV radiations consists of 3 major components UVA (320–400 nm, deep penetrating rays that contribute to premature skin aging and wrinkling), UVB(280–320 nm, less penetrating rays that induce skin reddening and sunburn) and

[1]College of Graduate Studies, UNESCO-UNISA Africa Chair in Nanosciences-Nanotechnology, Muckleneuk Ridge, PO Box 392, Pretoria, South Africa. [2]Nanosciences African Network (NANOAFNET), iThemba LABS-National Research Foundation, 1 Old Faure Road, PO Box 722, Somerset West 7129, Western Cape, South Africa. [3]Physics Deptartment, TUCAS Campus, Thiruvalluvar University Serkadu, Vellore 632115, India. [4]P.G. and Research Physics Department, A M Jain College, University of Madras, Meenambakkam, Tamil Nadu 600114, India. [5]Physics Department, University of Nottingham, Nottingham, UK. [6]IMMM, UMR 6283 CNRS, University of Le Maine, Bd O. Messiaen, 72085 Le Mans Cedex 09, France. [7]International Organization for Chemistry in Development, Liege, Belgium. ✉email: Ntombi.Ditlopo@dst.gov.za; Maazam@unisa.ac.za

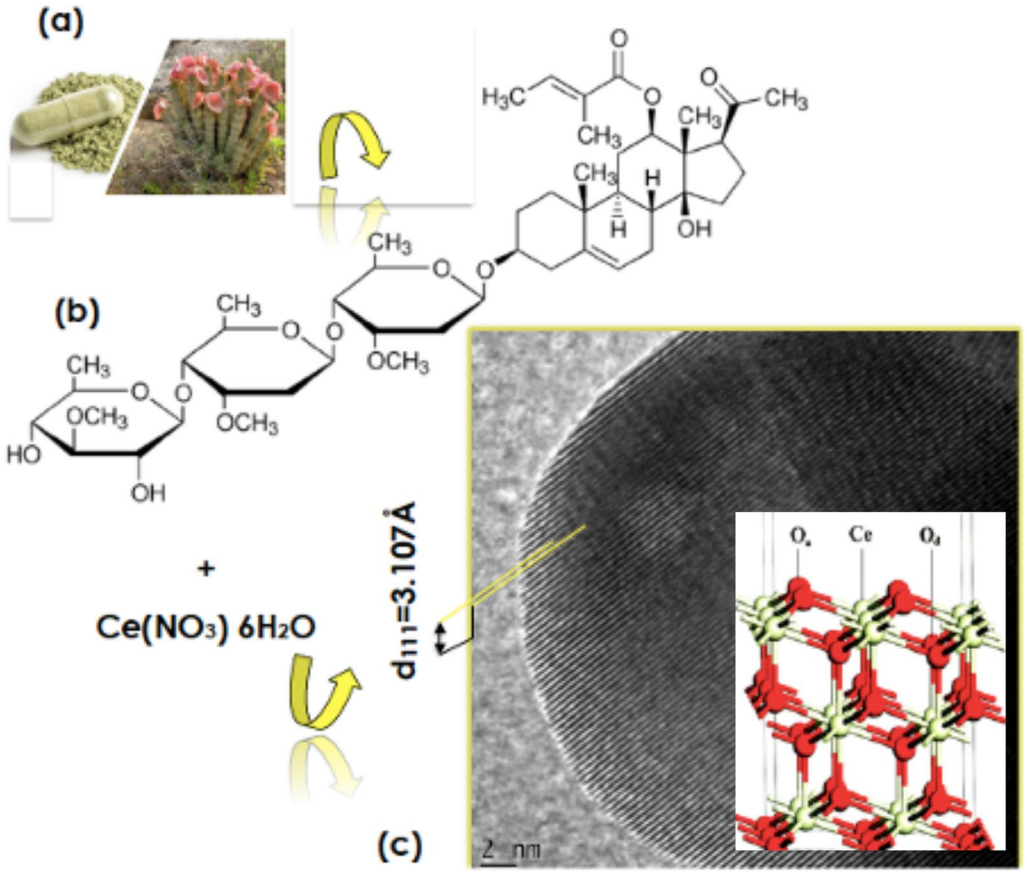

Figure 1. (**a**) Hoodia *gordonii* plant and in a powdered form, (**b**) chemical structure of the most active biocompound known as P57 (12-O-Trigloyl-3β,12β,14β-pregn-5-en-20-one3-O-β-D-thevetopyranosyl-(1 → 4)-β-D-cymaropyranosyl-(1 → 4)-β-D-cymaro-pyranoside), (**c**) typical HRTEM scan of a biosynthesized CeO_2 nanocrystal.

UVC(100–280 nm, most dangerous radiations but normally blocked by the earth's O_3 layer, O_2, and H_2O vapor present in the upper atmosphere of Earth). Figure 2b summarizes the various organic and inorganic major compounds available in the market as UV blocking sunscreens[13], namely; Octinoxate, Octisalate, Oxybenzone, Homosalate, Avobenzone, Octocrylene, TiO_2, ZnO.

As it will be sustained throughout the manuscript, the novelty and the originality of this contribution lie within the following major aspects:

(i) it is the first time within the scientific literature that Hoodia gordonii was used for the biosynthesis of nanoscaled CeO_2 in addition to the usage of hoodia gordonii as an appetite and thirst suppressant,
(ii) it is the first time that such a biosynthesized nano-CeO_2 exhibit a combined effective UV strong optical absorption, and a sound effectiveness against 2 major bacteria species, in addition to its minute ROS production relatively to standard oxides including TiO_2 and ZnO. This very low ROS production is of importance in minimizing the DNA induced damages,
(iii) Last but not least, this contribution sustains the importance of the indigenous knowledge and the valorization of anthropological aspects via scientifically supported studies.

Experiments and results

Biosynthesis methodology. For the biosynthesis typical phase, ground powder of Hoodia *gordonii* from Dischem South Africa was used. All used additional chemical reagents were purchased from Sigma-Aldrich. They were all of analytical grade, hence used without any additional purification. In a typical procedure, 10.0 g of clean Hoodia *gordonii* powder was weighed and mixed to 400 ml of deionized H_2O. The solution was kept at room temperature for about ~ 2 h. Thereafter, the obtained solution was filtered twice using Whatman filters to eliminate any residual solids. Following such a phase, 2.0 g of $Ce(NO_3)_3\,6H_2O$ was added to 100 ml of the filtered extract solution. The solution was then mixed under a thorough magnetic stirring and heated for ~ 2 h at about 48–50 °C. A solid precipitate was observed upon cooling. This deposit is likely to be CeOς or/and Ce(OH)ς or mixture of both. The solid deposit was purified by 2 repeated centrifugations at ~ 10,000 rpm for 10 min each. It was then dried in oven set at ~ 100 °C and thereafter annealed at various temperatures; 100, 200, 300, 400, 500, 700 °C for 2 h under air using a standard tubular furnace in view of crystalizing the likely CeOς/ Ce (OH)ς .

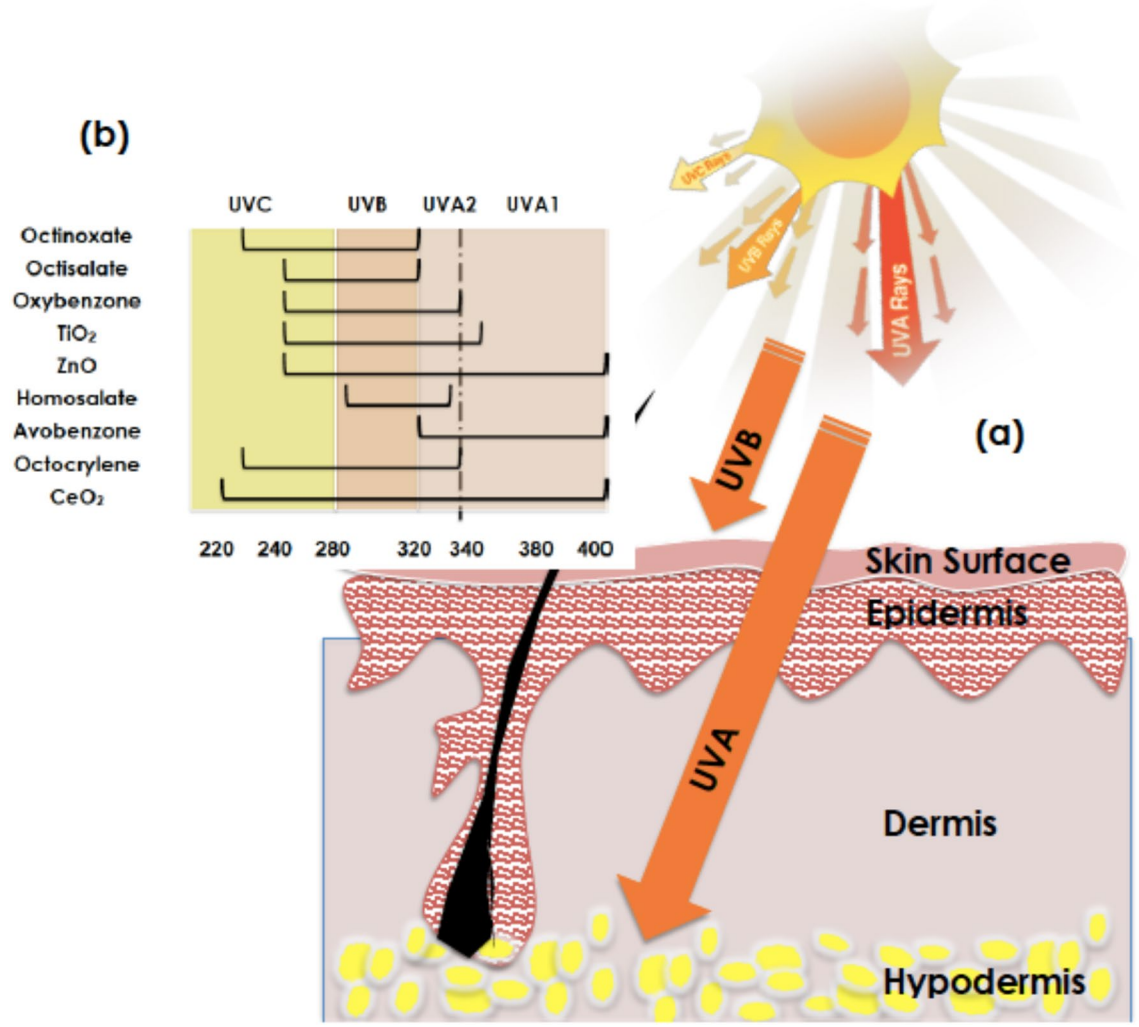

Figure 2. (**a**) Depth penetration of the various UV solar radiations within a human skin, (**b**) UV protection window of the current biosynthesized CeO_2 compared to those standard compounds (organics) and traditional nanoscaled oxides ZnO and TiO_2.

Morphology and crystalline atomic structure. Figure 3a–d report characteristic HRTEM micrographs and SAED patterns obtained on the CeOς/ Ce(OH)ς powder annealed at ~ 300 °C and ~ 700 °C respectively. in both cases, the particles are nano-scaled. The corresponding average size ⟨Ø⟩ of the particles (derived from a J-Image data treatment of the TEM images) ranges within 4.68–8.83 nm and 5.81–71.3 nm for the samples annealed at 300 °C and 700 °C respectively. Light scattering size analysis of Fig. 3e suggests a single mode size distribution for the annealed sample at 300 °C with likely an average size-centered at about 6.9 nm. It is however required to be cautious with such a value as we are at the limit of the DLS methodology. The annealed sample at 700 °C seems exhibiting a bimodal size distribution centered at 28.2 and 63.7 nm respectively**.** As one notices in Fig. 3a, the 300 °C annealed nano-powdered sample consists of agglomerates of various nano-crystals with different crystalline orientations as reflected by the polycrystalline nature of the SAED pattern of Fig. 3c. In contrast, for the ~ 700 °C annealed sample, the nanocrystals are larger but still in the nanoscale while significantly crystalline (Fig. 3b) in agreement with the spot type electron diffraction pattern of Fig. 3d. In both cases, the indexation of the annular and singular diffraction patterns is in agreement with the face centered cubic phase of CeO_2 (JCPDS 34–0394) corresponding to an average lattice constant of $\langle a \rangle = 3.865$ Å which is the most reflecting reticular plans'distance $d_{111} = 3.107$ Å. More accurately, this later crystallographic phase consists of a cubic fluorite-type oxide in which each Ce site is surrounded by 8 O sites in an fcc arrangement while each O site occupies a tetrahedron Ce site. This seems to be in agreement with the X-Rays diffraction investigations of Fig. 3f. The following Bragg diffractions peaks are observed; (111), (220), (220), (311) as well as (222). Such a diffraction pattern fits with the single-phase Fluorite of polycrystalline CeO_2. However, It is worth noting that each and all Bragg peaks' angular position seem to shift towards higher angles relatively to those of the 300 °C annealed sample. Such an angular shift is relatively small of the order of $4.36\ 10^{-3}$ rad between the 300 °C (Smaller nanocrystals) and 700 °C (Larger nanocrystals). Hence all reticular atomic diffraction plans of the smaller nanocrystals especially will likely be submitted to a compression comparatively to the bulk. Such a relative compression is $\Delta d/d = (\cos \Theta / \sin \Theta)\Delta\Theta$. In the case of the nanocrystals of the CeO_2 sample annealed at 300 °C, such a relative

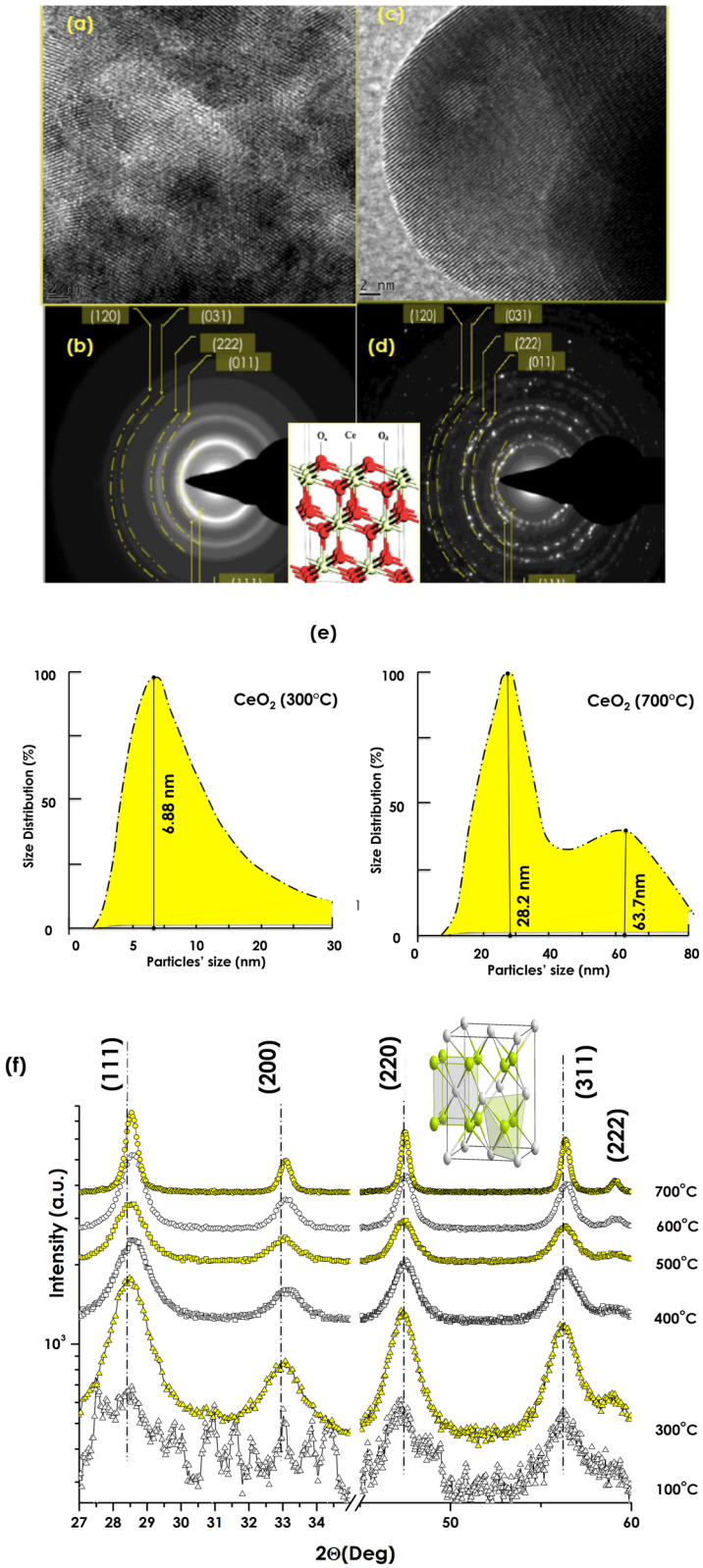

Figure 3. HRTEM of the CeO_2 powder and annealed at ~ 300 °C (**a**) and ~ 700 °C (**c**) respectively and their corresponding SAED (**b**,**d**), DLS size distribution (**e**) and the XRD spectra of the various samples (**f**).

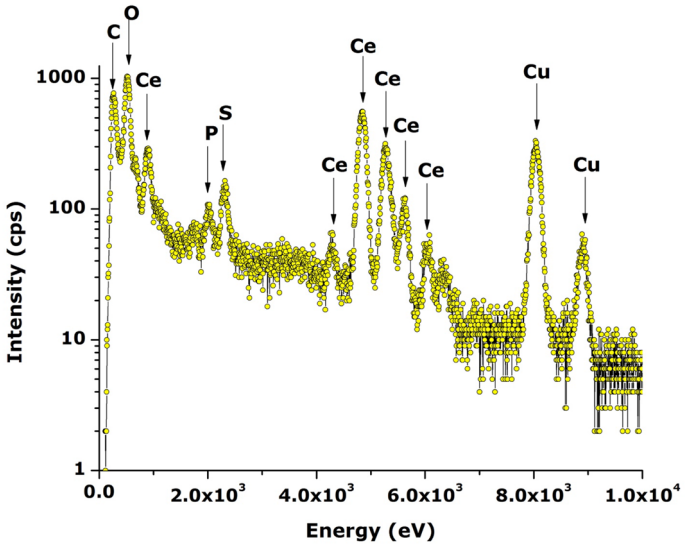

Figure 4. Representative EDS spectrum of CeO_2 nano-powder annealed at ~ 700 °C.

contraction Δd/d variation is of the order 6.014 10^{-3} induced likely by surface tension phenomena as it is the case in nanocrystals in general.

Elemental analysis and surface coordination. Figure 4 shows a representative EDS elemental analysis spectrum in logarithmic intensity to put in evidence any potential contamination during the biosynthesis phase. As one can notice, excluding the carbon originating from the Carbon coated grid, there are no other elements observed except Cerium (Several peaks in relation to the f-electrons nature of Ce and Oxygen in addition to Sulfur and Potassium. These later ones, i.e. sulfur (S) and phophorus (P) originate likely from the natural extract's organic compounds as it was observed previously in the case of several biosynthesis of several nan-oxides[2,14]. However, it is to be highlighted that the limit of detection of EDS being of the order of 10%, other contaminants can not be excluded if their concentration is below the 10% limit.

Likewise, the XPS studies of the annealed CeO_2 nanoparticles were performed to investigate precisely the oxidation state of Ce and O (Fig. S1). The binding energy of CeO_2 nanoparticles exhibited several bands with the main ones centered at about 882.2, 888.5, 897.7 and 916.3 eV corresponding to the Ce^{4+} 3d3/2 and Ce^{4+} 3d5/2 in addition to the O1s peak at 531 eV. The XPS observations are consistent with the reported values in the literature[14–18]. Hence, one can conclude that Ce is likely to be in 4 + valence state.

UV Optical selectivity. Figure 5a reports the diffuse Reflectivity of the nanoscaled CeO_2 pressed powder samples annealed at various temperatures. One can distinguish 2 major trends. The sample annealed at 100 °C and those above exhibit stringently different spectral variations. While the diffuse reflectance varies approximately in a linear way with the wavelength for the sample annealed at 100 °C, those above exhibit a Heaviside-like function variation with the wavelength and a wavelength cut-off at the vicinity of $\lambda_{cut\text{-}off} \sim 400$ nm. Above such a wavelength, the diffuse reflectance reaches promptly a plateau in the VIS and NIR spectral regions. This Heaviside function-like variation is close comparable to a perfect selectivity response as represented by the dashed yellow curve in Fig. 5a. Higher is the annealing temperature, higher is the plateau. The average value of the plateau of Reflectivity varies from 45 to 63% for samples annealed within 300–700 °C temperature range with a significantly low reflectivity in the UV-Bleu i.e. below $\lambda_{cut\text{-}off} \sim 400$ nm. In this UV spectral region, the reflectivity exhibits a significant fluctuation with an average of 0.7%. Because of the opacity of the CeO_2 pellet and low reflectivity in this range, the UV selectivity is likely to be absorption dominated. This UV absorption is likely to be governed mainly by the transition of O 2p2 – to Ce 4f. 4 + as schematically represented in Fig. 5b. The optical transmission of thin pellets (thickness < 0.1 mm) of the various samples is reported in Figure S.2). As one can notice, the optical transmission is significantly low within the limit of detection both in the UV and bleu spectral regions. It can safely be deduced the absorption in the UV spectral region A = 1-R-T is dominant (A ~ 100%).

ROS activity and photostability studies. In relation to the UV ROS photostability, Fig. 5c displays the relative Reactive Oxygen Species (ROS) production versus concentration of the biosynthesized nano-CeO_2 as well as that of standard nano-TiO_2 used as a reference for comparison. While the ROS production of nano-TiO_2 increases significantly with the concentration reflecting its elevated photoactivity. In contrast, the ROS production of the biosynthesized nano-CeO_2 seems stabilizing at very low values over the investigated concentration range of 0.5–1000 µg/ml. This high photostability is, likely, to be correlated to the high stoichiometry of the biosynthesized CeO_2 and the Ce4 + dominant valency in agreement with the XPS studies. Any non-stoichiometry in CeO_2 arising from O deficiency both surface or in volume would be responsible for the production of free charge carriers upon UV irradiation and hence a ROS increase. The faster recombination rate of any generated

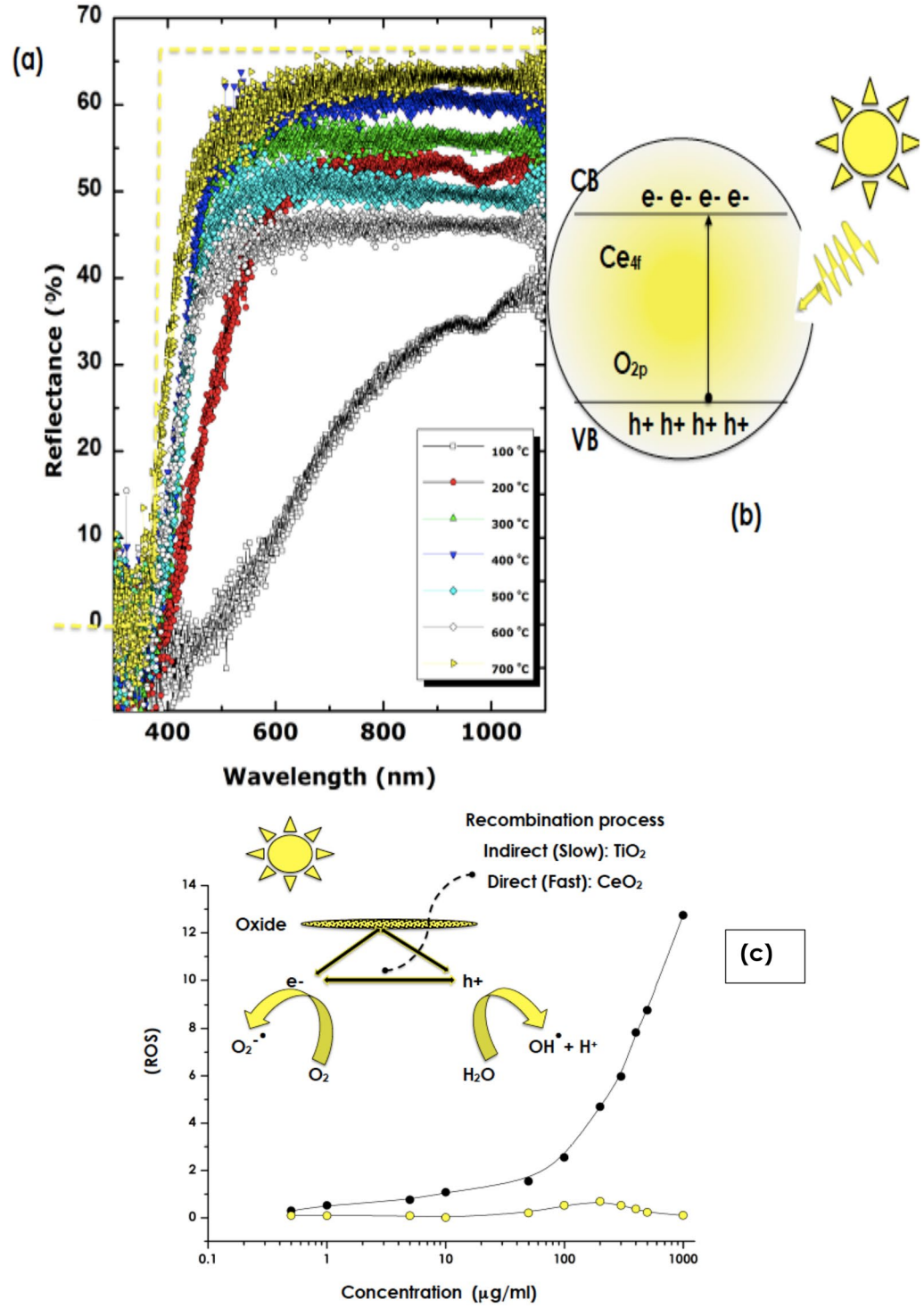

Figure 5. (**a**) Diffuse Reflectivity of the CeO_2 annealed at various temperatures within the range of 100–700 °C, (**b**) band structure and the potential O 2p2 – to Ce 4f. 4 + transitions, (**c**) ROS production of the 700 °C annealed CeO_2 (yellow circles) and standard nanoTiO_2 (black closed circles), and inset (**b**) schematic representation of the e–h creation/recombination in TiO_2 and CeO_2.

e–h pairs in CeO_2 relatively to that of TiO_2 could explain such a low rate of ROS production[9,11,12]. In addition, there is a need to investigate the photostability as this parameter is of a pivotal role[19,20]. Accordingly, photostability studies were conducted using standard UV illuminations with long exposure time of 120 min. For such, a Solar Light's advanced Model 601 Multiport® SPF Testing Solar Simulator was used. It is the industry standard for high throughput SPF testing and dermatological studies. It produces UVA or UVA + B (290–400 nm)/300 W. The samples were exposed to UVA + B during 120 min each with a 2 cm beam spot. The diffuse reflectivity was

measured before and after such UVA + B irradiations. Figure S.3 reports the reflectivity of the 300 °C and 700 °C annealed samples before and after the UVA + B irradiations. As one can notice, and excluding the statistical fluctuations, there is nearly no significant change in the reflectivity profiles. Consequentially, it is safe conclude on the UVA + B photostability of the biosynthesized nano-CeO_2. Such a photostability could be linked to the dominant Ce4 + valence and/or absence of oxygen deficiencies. Nonetheless, it is necessary to reconduct such a study once the nano CeO_2 nanoparticles are embedded in a standard formulation for real life cosmetic applications.

Conclusion

In summary, this study validated the efficiency of Hoodia *gordonii* natural extract as an effective agent for the biosynthesis of single phase CeO_2 nanocrystals. Such bio-engineered nanocrystals exhibited a remarkable UV filtering optical selectivity quasi-similar to a perfect UV filtering system. In view of their negligible reactive oxygen species production, such a UV selectivity is conjugated to an exceptional photostability (Relative ROS < 0.5). Relatively to ordinary nanoscaled TiO_2 and ZnO used in standards cosmetics, The currently bio-engineered CeO_2 exhibited a superior photostability correlated to a low formation of harmful reactive intermediates such as singlet oxygen and reactive oxygen species (ROS) including Hydroxyl radicals which not only damage the DNA plasmids but also the skin cells. in support of their potential application novel green UV protective nanocosmetics specifically, and skin protection in general. Nonetheless, it is necessary to reconduct such a study once the nano CeO_2 nanoparticles are embedded in a standard formulation for real life cosmetic applications.

Received: 31 July 2021; Accepted: 1 February 2022
Published online: 02 March 2022

References

1. Sweet, R. *"Hortus Britannicus" 1783–1835* (J. Ridgeway, Smithsonian Libraries, 1830).
2. Diallo, A., Doyle, T. B., Park, E. & Maaza, M. Green synthesis of Co_3O_4 nanoparticles via *Aspalathus linearis*: Physical properties. *Green Chem. Lett. Rev.* **8**(3–4), 30–36 (2015).
3. Kasinathan, K., Kennedy, J., Elayaperumal, M. & Henini, M. Photodegradation of organic pollutants RhB dye using UV simulated sunlight on ceria based TiO_2 nanomaterials for antibacterial applications. *Sci. Rep.* **6**, 38064 (2016).
4. Minami, Y., Yin, S. & Sato, T. Cerium oxide for sunscreen cosmetics. *J. Solid State Chem.* **171**, 7–11 (2003).
5. Wu, Y. *et al.* Proton transport enabled by a field-induced metallic state in a semiconductor heterostructure. *Science* **369**(6500), 184–188 (2020).
6. Cargnello, M. *et al.* Exceptional activity for methane combustion over modular Pd@CeO_2 subunits on functionalized Al_2O_3. *Science* **337**(6095), 713–717 (2012).
7. Nie, L. *et al.* Activation of surface lattice oxygen in single-atom Pt/CeO_2 for low-temperature CO oxidation. *Science* **358**(6369), 1419–1423 (2017).
8. Campbell, C. T. *et al.* Oxygen vacancies and catalysis on ceria surfaces. *Science* **309**(5735), 713–714 (2005).
9. Chueh, W. C. *et al.* High-flux solar-driven thermochemical dissociation of CO_2 and H_2O using nonstoichiometric ceria. *Science* **330**, 1797–1801 (2020).
10. Ivanov, V. K. *et al.* Structure-sensitive properties and biomedical applications of nanodispersed cerium dioxide. *Russ. Chem. Rev.* **78**(9), 855–871 (2009).
11. Parwaiz, S. *et al.* CeO_2-based nanocomposites: An advanced alternative to TiO_2 and ZnO in sunscreens. *Mater. Express* **9**, 185–202 (2019).
12. Serpon, N. *et al.* Inorganic and organic UV filters: Their role and efficacy in sunscreens and suncare products. *Inorg. Chim. Acta* **360**, 794 (2007).
13. Federal Register 64 27666, *Sunscreen Drug Products for Over-the-Counter Human Use, Final Monograph* (US Food and Drug Administration, 2000).
14. Thovhogi, N. *et al.* Nanoparticles green synthesis by Hibiscus Sabdariffa flower extract: Main physical properties. *J. Alloys Compd.* **647**, 392–396 (2016).
15. He, L. *et al.* Highly bioactive zeolitic imidazolate framework-8–capped nanotherapeutics for efficient reversal of reperfusion-induced injury in ischemic stroke. *Sci. Adv.* **6**(12), eaay9751 (2020).
16. Hao, P. *et al.* Controlling information duration on rewritable luminescent paper based on hybrid antimony(III) chloride/small-molecule absorbates. *Sci. Adv.* **6**(20), eabc2181 (2020).
17. Faure, B. *et al.* Dispersion and surface functionalization of oxide nanoparticles for transparent photocatalytic and UV-protecting coatings and sunscreens. *Sci. Technol. Adv. Mater.* **14**, 023001 (2013).
18. Li, Z. X. *et al.* Sustainable and facile route to nearly monodisperse spherical aggregates of CeO_2 nanocrystals with ionic liquids and their catalytic activities for CO oxidation. *J. Phys. Chem. C* **112**, 18405 (2008).
19. Garbe, B. *et al.* The influence of short-wave and long-wave radiation spectrum on the photostability of sunscreens. *Skin Pharmacol. Physiol.* **33**(2), 77–85. https://doi.org/10.1159/000505218(2020) (2020).
20. Gonzalez, H. *et al.* Photostability of commercial sunscreens upon sun exposure and irradiation by ultraviolet lamps. *BMC Dermatol.* https://doi.org/10.1186/1471-5945-7-1(2007) (2007).

Acknowledgements

This research program was generously supported by grants from the University of South Africa (UNISA) (Grant No. UNISA-U2ACN2-2021), the National Research Foundation of South Africa (NRF), iThemba LABS, the French Ministry of Europe & Foreign Affairs via the ADESFA II program), the Organization of Women for Science the Developing World (OWSD) and Abdul Salam ICTP via the Nanosciences Africa Network (NANOAFNET) as well as the African Laser Centre (ALC) to whom we are grateful.

Author contributions

N.D.: Samples Preparation, Associated to various experiments & data analysis & Manuscript writing. N.S.: Samples preparation. S.K.: Optical characterization & Analysis. E.M. & K.G.: ROS investigations & analysis. M.H.: Data analysis & Manuscript writing. A.G.: Data analysis & interpretation. A.K.: Phytochemistry guidance & experimental optimization. M.M.: Conceptualization, data analysis, interpretation & manuscript writing.

Competing interests
The authors declare no competing interests.

Additional information
Supplementary Information The online version contains supplementary material available at https://doi.org/10.1038/s41598-022-06828-x.

Correspondence and requests for materials should be addressed to N.D. or M.M.

Reprints and permissions information is available at www.nature.com/reprints.

Publisher's note Springer Nature remains neutral with regard to jurisdictional claims in published maps and institutional affiliations.